AIAA AVIATION Forum
12-16 June 2023, San Diego, CA and Online
AIAA AVIATION 2023 Forum

10.2514/6.2023-3651

Bispectral mode decomposition of axisymmetrically and non-axisymmetrically forced turbulent jets

Akhil Nekkanti * and Oliver T. Schmidt†
University of California San Diego, La Jolla, CA USA

Igor A Maia‡ and Peter Jordan§
Institut Pprime-CNRS-Université de Poitiers-ENSMA, Poitiers France

Liam Heidt ¶ and Tim Colonius ‖
California Institute of Technology, Pasadena, CA USA

Large-eddy simulations (LES) of a turbulent unforced jet at $Re = 50,000$ and $M_j = 0.4$, and jets forced at azimuthal wavenumbers $m = 0$, $m = \pm 1$, $m = \pm 2$ and $m = \pm 6$ are performed. The objective of this study is to characterize the nonlinear interactions that are initiated by the forcing. To achieve this, we used the bispectral mode decomposition (BMD) technique, which is tailored to extract flow structures associated with triadic interactions. Azimuthal wavenumber triads are investigated using the cross-spectral variant of BMD. Axisymmetric forcing generates peaks at the forcing frequency and its harmonics in the $m = 0$ component only, whereas non-axisymmetric forcing generates peaks at different azimuthal wavenumbers. The latter aspect is investigated using cross-BMD. Forcing the jet at $m = \pm 1$, the only odd-m forcing case considered, creates a cascade of triads that generates peaks at the forcing frequency and its odd harmonics at odd azimuthal wavenumbers and even harmonics at even azimuthal wavenumbers. Forcing the jet at $m = \pm m_f$ azimuthal wavenumbers produces peaks at the odd harmonics in the odd integer multiples of m_f and at even harmonic frequencies in the even integer multiples of m_f.

I. Introduction

The reduction of jet noise is an important objective for the aviation community. The pioneering work by Crow and Champagne [1] identified the presence of large-scale coherent structures in turbulent jets, and these coherent structures or wavepackets are the primary sources of aft-angle noise [2]. Following Crow and Champagne [1], harmonically-forced jets have been the subject of numerous studies, for example, [3–8]. The actuation of the jet has varied over a wide range of frequencies and forcing amplitudes. At low amplitudes of forcing, the jets exhibit a linear response. As the forcing amplitude increases, it triggers nonlinear interactions in jets. High levels of forcing and the resulting nonlinear interactions of coherent structures have rarely been explored. Previous studies [9–11] have investigated the nonlinear response to high amplitude forcing in jets, and most have focussed on initially-laminar jets.

Harmonic forcing induces a phase-locking mechanism that simplifies the eduction of coherent structures. Most studies that involve the excitation of a jet employ axisymmetric forcing. Only a few studies have investigated the effect of non-axisymmetric forcing, such as [12–16]. Cohen and Wygnanski [12] and Long and Petersen [13] forced the jet at the same frequency but opposite wavenumbers to demonstrate that the jet loses its azimuthal symmetry, producing elliptical and square cross-sections. Samimy et al. [15] forced the jet at various azimuthal wavenumbers and found that $m = \pm 1$-forcing provides the maximum mixing enhancement and shortest potential core length. Wu and Huerre [17] hypothesized that the interaction of a helical conjugate pair with $m = \pm 1$ generates a slowly modulating mean-flow

*PhD Student, Department of Mechanical and Aerospace Engineering, AIAA Student Member
†Assistant Professor, Department of Mechanical and Aerospace Engineering, Senior Member AIAA.
‡Post-Doctoral Research Fellow, Département of Fluides Thermique et Combustion, Institut Pprime-CNRS-Université de Poitiers-ENSMA, Poitiers France.
§Directeur de Recherche, Département of Fluides Thermique et Combustion, Institute Pprime-CNRS-Université de Poitiers-ENSMA, Poitiers France.
¶PhD Student, Graduate Aerospace Laboratories of the California Institute of Technology, AIAA Student Member
‖Frank and Ora Lee Marble Professor of Mechanical Engineering, Mechanical and Civil Engineering, Associate Fellow AIAA

distortion. They further show that this interaction radiates low-frequency sound to jet angles between 45°-60°. Using numerical simulations, Suponitsky et al. [18] reported similar findings.

In this work, we perform LES of unforced and forced turbulent subsonic jets at a Reynolds number, $Re = \rho_j U_j D/\mu_j = 50,000$, and Mach number, $M = U_j/c_\infty = 0.4$, where ρ is the density, U the mean flow velocity, μ the dynamic viscosity, c the speed of sound, and the subscripts j and ∞ denote the jet and free-stream conditions. The jets are forced harmonically at a non-dimensional frequency of $St_f = fD/U_j = \omega D/2\pi U_j = 0.4$ and different azimuthal wavenumbers, $m = 0$, $m = \pm 1$, $m = \pm 2$, and $m = \pm 6$ near the nozzle lip. The objective of this work is to characterize the nonlinear interactions triggered by the excitation of the jet. To accomplish this, we employ the bispectral mode decomposition (BMD) technique proposed by Schmidt [19]. BMD extracts the spatial flow structures generated through triadic interactions and identifies the most dominant triads in the flow by maximizing the spatially-integrated bispectrum. BMD has been used to investigate the triadic interactions in various flow configurations, such as laminar-turbulent transition on a flat plate [20], forced jets [21, 22], swirling flows [23], bluff body wakes [24], and wake of an airfoil [25]. Forcing the jet harmonically also generates phase-dependent coherent structures that are slaved to the forcing which can be extracted by the cyclostationary spectral proper orthogonal decomposition (CS-SPOD) [26].

The paper is organized as follows. In section II, the BMD methodology is discussed. In section III, the simulations are validated against companion experiments. In section IV, the results are presented and the work is summarized in section V.

II. Bispectral mode decomposition

BMD is a technique that can be understood as an extension of classical bispectral analysis to multidimensional and multivariate data. The bispectrum is defined as the double Fourier transform of the third moment of a time signal. For a time series, $y(t)$ with zero mean, the bispectrum is

$$S_{yyy}(f_1, f_2) = \int\int R_{yyy}(\tau_1, \tau_2) e^{-i2\pi(f_1\tau_1 + f_2\tau_2)} d\tau_1 d\tau_2, \tag{1}$$

where $R_{yyy}(\tau_1, \tau_2) = E[y(t)y(t-\tau_1)y(t-\tau_2)]$ is the third moment of $y(t)$, and $E[\cdot]$ is the expectation operator. The bispectrum is a signal processing tool for one-dimensional time series which only measures the quadratic phase coupling locally. On the contrary, BMD is a modal decomposition technique that identifies the spatially coherent structures associated with the triadic interactions.

For a fluctuating flow field $\mathbf{q}_i = \mathbf{q}(x, t_i)$, where $i = 1, 2, \cdots n_t$, BMD maximizes the integrated point-wise bispectrum

$$b(f_k, f_l) = E\left[\int_\Omega \hat{\mathbf{q}}^*(x, f_k) \circ \hat{\mathbf{q}}^*(x, f_l) \circ \hat{\mathbf{q}}(x, f_k + f_l) dx\right]. \tag{2}$$

Here, $\hat{\mathbf{q}}$ is the temporal Fourier transform of $\mathbf{q}$ computed using the Welch approach [27], Ω is the spatial domain of interest, $(\cdot)^*$ denotes the complex conjugate, and $\circ$ denotes the Hadamard (or element-wise) product.

Next, all the Fourier realizations at frequency f_k are arranged into a matrix, $\hat{\mathbf{Q}}_k = \left[\hat{\mathbf{q}}_k^{(1)}, \hat{\mathbf{q}}_k^{(2)}, \cdots, \hat{\mathbf{q}}_k^{(n_{blk})}\right]$. The auto-bispectral matrix is then computed as

$$\mathbf{B} = \frac{1}{n_{blk}} \hat{\mathbf{Q}}_{k\circ l}^H \mathbf{W} \hat{\mathbf{Q}}_{k+l}, \tag{3}$$

where $\hat{\mathbf{Q}}_{k\circ l}^H = \hat{\mathbf{Q}}_k^* \circ \hat{\mathbf{Q}}_l^*$ and $\mathbf{W}$ is the diagonal matrix containing the spatial quadrature weights. Owing to the non-Hermitian nature of the bispectral matrix, we obtain the complex mode bispectrum by solving the optimization problem

$$\lambda_1(f_k, f_l) = \arg\max \left| \frac{\mathbf{a}_1^* \mathbf{B} \mathbf{a}_1}{\mathbf{a}_1^* \mathbf{a}_1} \right|, \tag{4}$$

for the optimal expansion coefficients $\mathbf{a}_1$, by determining the numerical radius of $\mathbf{B}$. For further details on computing the mode bispectrum, the reader is referred to Schmidt [19]. Finally, the bispectral modes and the cross-frequency fields are recovered as

$$\boldsymbol{\phi}_{k+l}^{(1)} = \hat{\mathbf{Q}}_{k+l} \mathbf{a}_1, \quad \text{and} \tag{5}$$

$$\boldsymbol{\phi}_{k\circ l}^{(1)} = \hat{\mathbf{Q}}_{k\circ l} \mathbf{a}_1, \tag{6}$$

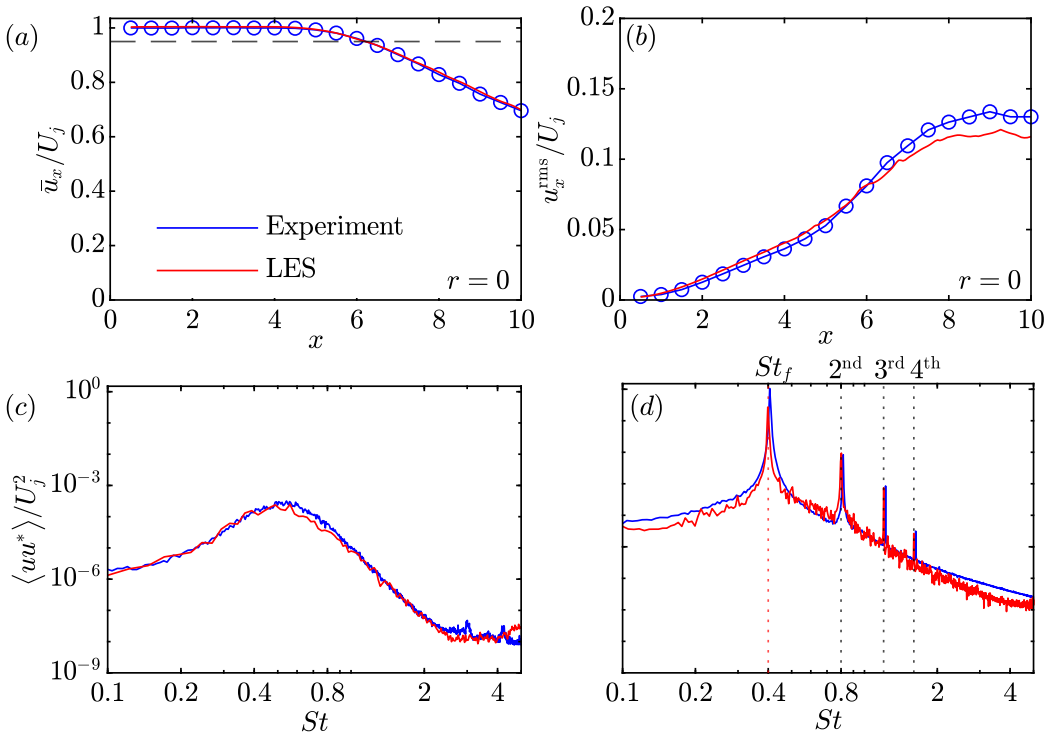

Fig. 1 Comparison of the experiment with the LES simulations: (a-c) unfoced jet; (d) forced jet. Profiles of the mean (a) and RMS (b) streamwise velocity on the centerline. Power spectral density (c, d) of the streamwise velocity at $x = 2$ and $r = 0$. The experiment (blue line) is compared to the simulations (red line). Black dashed line represents $U/U_j = 0.95$ and its intersection with the mean streamwise velocity indicates the length of the potential core. $St = St_f = 0.4$ corresponds to the forcing frequency (red dotted line) [22].

respectively. By construction, the bispectral modes and cross-frequency fields have the same set of expansion coefficients. The complex mode bispectrum, λ_1, measures the intensity of the triadic interaction and the bispectral mode, $\boldsymbol{\phi}_{k+l}$, represents the structures that results from the nonlinear triadic interaction.

In this study, we use the cross-spectral variant of BMD to measure the interaction between different azimuthal wavenumbers. Here, the azimuthal wavenumber triplets will be represented using $[\cdot,\cdot,\cdot]$ and all the frequency triads will be represented using $(\cdot,\cdot,\cdot)$.

III. Validation of LES

The experiments of the isothermal subsonic jets were performed at the "JET100" low Mach number jet facility at Institut PPRIME, Poitiers, France. The experiments were carried out for a jet Mach number M_j = 0.05, and Reynolds number of $Re = 50000$. The boundary layer is tripped inside the nozzle by a carborundum strip located $2.5D$ upstream from the nozzle exit. The turbulent jet is forced by eight loudspeakers that are equally distributed around the nozzle lipline ($r/D = 0.5$). The loudspeakers generate synthetic jets through an annular gap of width $0.01D$. For further details of the experimental setup, the reader is referred to Maia et al. [28, 29, 30].

We perform large-eddy simulations of subsonic jets using the compressible flow solver "Charles" developed at Cascade Technologies [31, 32]. Charles solves the spatially filtered compressible Navier–Stokes equations on unstructured grids using a density-based finite-volume method. The LES combines the Vreman sub-grid model [33] with the wall-model by Bodart and Larsson [34, 35]. The reader is referred to Brès et al. [31, 32] for further details on the numerical method and validation on jet flows.

The validation of the LES case for the present case follows the previous studies. In particular, the mesh used by Brès et al. [32] is modified to accommodate the new nozzle geometry and refined in the vicinity of the synthetic jet actuators. The total grid size is 16.6 million control volumes. The LES is conducted for the experimental Reynolds number, whereas the Mach number is artificially increased to $M_j = 0.4$. Effects of compressibility are still small in this

regime and the very small time steps associated with the incompressible limit are avoided.

The LES results for the unforced jet are compared to the experiments in figure 1. The mean and RMS streamwise velocities on the centerline and lipline are reported in Fig. 1(a,c) and 1(b,d), respectively. In Fig. 1(a), the mean streamwise velocities along the centerline of the experiment and the simulation are almost indistinguishable within the first ten jet diameters. The corresponding potential core length, indirectly defined as $\bar{u}(x = x_c) = 0.95U_j$ is $x_c \approx 6.2$. The RMS velocity along the centerline, shown in Fig. 1(c), matches well for the first six jet diameters and is underpredicted by about 10% further downstream. Clearly visible in the simulation results are grid transitions that were similarly observed by Brès et al. [32]. It was confirmed in the same work that increasing the resolution mitigates these transitions. More importantly, Brès et al. [32] also showed that both nozzle-exit turbulent statistics and far-field noise predictions were accurate for the lower resolution simulations that exhibit grid transitions.

For the forced simulations, we follow Heidt et al. [36] and model the effect of the loudspeaker actuators as an acoustic forcing in the annular region along the lip line, $0.50 \leqslant r \leqslant 0.51$, as

$$p(r) = 1 - 40000(r - 0.505)^2, \tag{7a}$$

$$u_x(r,t) = Ap(r)\cos\left(m_f\theta\right)\sin\left(2\pi St_f t\right), \tag{7b}$$

$$u_r = u_\theta = 0, \tag{7c}$$

$$\rho = \rho_\infty + \rho_\infty u_x/c_\infty, \tag{7d}$$

$$p = p_\infty + \rho_\infty c_\infty u_x. \tag{7e}$$

The amplitude, A, was manually adjusted to match the experimental observations. Here, $St_f = 0.4$ is the forcing frequency. Fig. 1(c,d) shows the power spectral densities of the centerline streamwise velocity at $x = 2$ for the unforced and axisymmetrically forced jets. The comparison between experiment and simulation are excellent for the unforced jet seen in Fig. 1(c). The best agreement for the forced case was obtained for $A = 0.4$ and is shown in Fig. 1(d). Both the peaks at the forcing frequency and its harmonics, as well as the number of active harmonics and the underlying broadband spectrum, are well predicted.

IV. Results

Figure 2 shows the area-integrated power spectral densities (PSD) for the five most energetic azimuthal wavenumbers $m = 0, 1, 2, 3, 4$. The PSDs are integrated over the compressible energy norm. The azimuthal wavenumber $m = 1$ contains most of the energy for the unforced jet. For the axisymmetrically forced jet, we observe large peaks at the forcing frequency and its harmonics in the wavenumber $m = 0$. The peaks at these harmonic frequencies indicate the presence of triadic sum interactions. For the $m = \pm1$-, $m = \pm2$-, and $m = \pm6$- forced jets, peaks are observed at the odd harmonics $St = St_f, 3St_f, \cdots$, in the actuated azimuthal components, i.e., $m = 1$,$m = 2$ and $m = 6$, respectively. Peaks exist at the even harmonics ($St = 2St_f, 4St_f, 6St_f, \cdots$) in $m = 0, 2, 4$ for the $m = \pm1$-forced jet, in $m = 0, 4, 8$ for the $m = \pm2$-forced jet, and in $m = 0, 12, 24$ for the $m = \pm6$-forced jet. These observations indicate that the triadic interactions occur in both the frequency and azimuthal wavenumber space for non-axisymmetrically forced jets.

The mode bispectra for the $m = 0$ component of the unforced and forced jets are shown in Fig. 3. The high-intensity regions (false red color) in the mode bispectra signify the dominant triads that arise from the interactions of two frequencies. Different combinations of frequencies (St_1,St_2) interact to generate the same frequency ($St_1 + St_2$ = constant) along the diagonals of slope -1 in the mode bispectrum. For the forced jet (figure 3 (b)), a grid-like pattern is observed with vertical, horizontal, and diagonal lines at the forcing frequency and its harmonics with local maxima at the intersection of these lines. These local maxima represent the prominent triadic interactions. In particular the two most dominant triads are (0.4,0.4,0.8) and (0.8,-0.4,0.4), denoted by circles in the figure inset. The latter triad indicates a back-scatter effect where energy is supplied to the fundamental by the second harmonic. In the case of unforced jets, a broadband behavior is observed, with the highest values concentrated at lower frequencies.

For non-axisymmetrically forced jets, peaks exist in multiple azimuthal wavenumbers, which indicates the interactions between different azimuthal wavenumbers. Hence, we compute the cross-BMD to characterize these triadic interactions. Fig. 4 shows the cross-mode bispectra for the $m = \pm1$ forced jet. Here, we show five azimuthal triplets, [m_1,m_2,m_3] = [1,-1,0], [1,1,2], [2,1,3], [2,2,4], and [3,1,4], where $m_1 + m_2 = m_3$. For the [1,-1,0] triplet, the cross-bispectra is symmetric about the lines, $St_1 = St_2$ and $St_1 = -St_2$. For the triplets, [1,1,2] and [2,2,4], the cross-bispectra is symmetric about the line $St_1 = St_2$, whereas there is no symmetry for the triplets, [2,1,3] and [3,1,4]. These symmetry lines are denoted using white dash-dotted lines. Fig. 4(a) shows the interaction of helical component ($m = 1$)

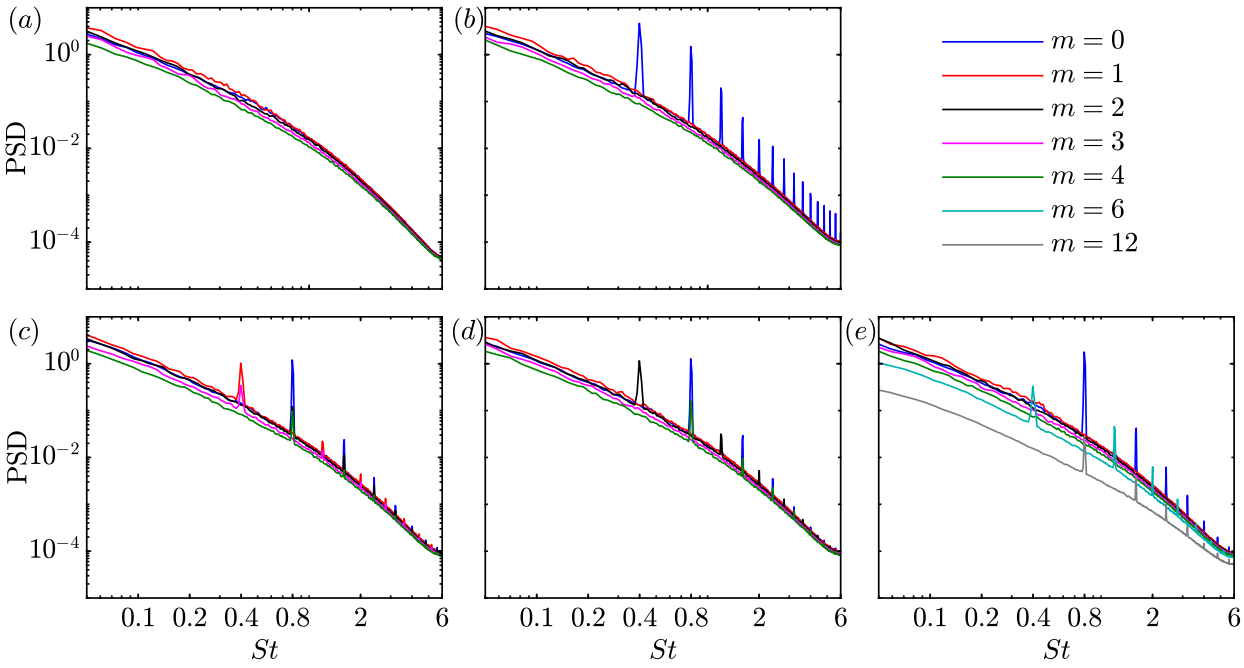

Fig. 2 Integrated PSD of first five azimuthal wavenumbers, $m = 0, 1, 2, 3, 4$ for the four jets: (a) unforced; (b) axisymmetrically forced; (c) $m = \pm 1$-forced; (d) $m = \pm 2$-forced; (e) $m = \pm 6$-forced jet. In (e) $m = 6, 12$ are also shown. PSD is integrated over the compressible energy norm.

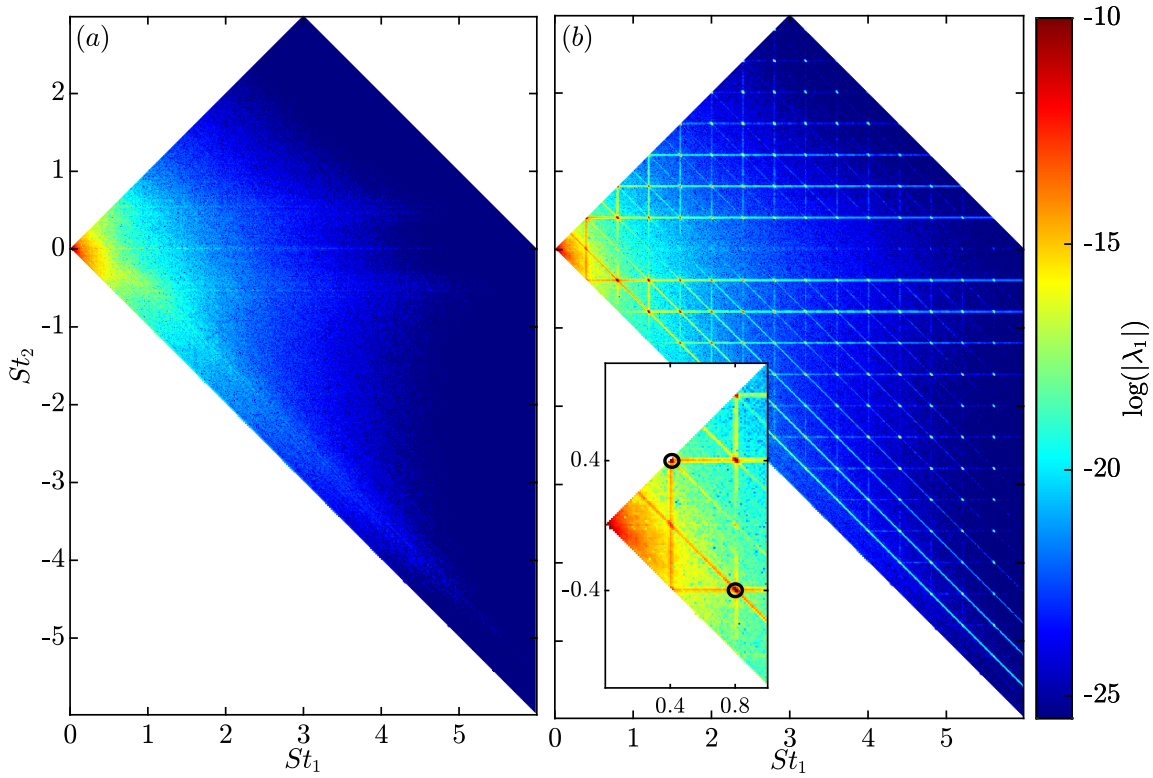

Fig. 3 BMD spectra: (a) unforced turbulent; (b) axisymmetrically forced turbulent jet.

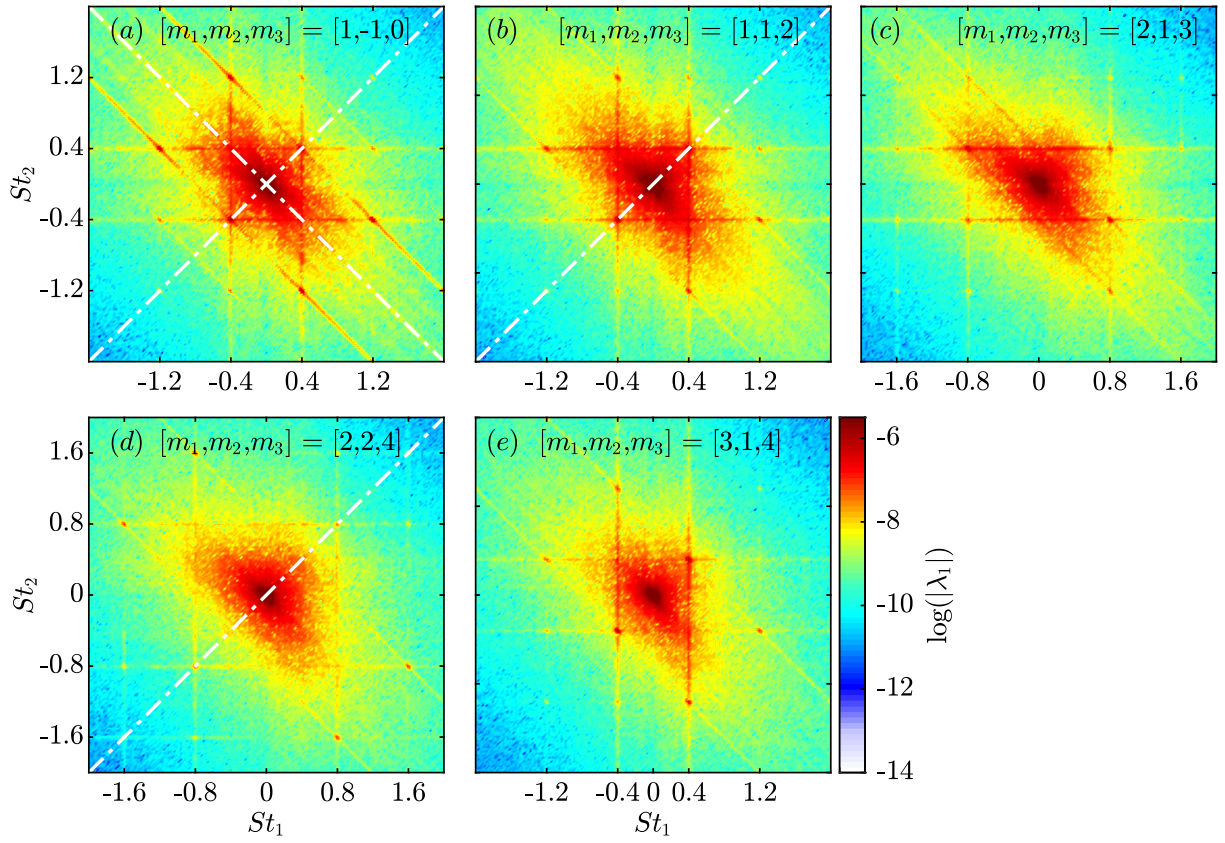

Fig. 4 Cross-BMD spectra that shows the interaction of the azimuthal wavenumbers triads, [m_1, m_2, m_3], for the forced $m = \pm 1$ jet: (*a*) [1,-1,0]; (*b*) [1,1,2]; (*c*) [2,1,3]; (*d*) [2,2,4]; (*e*) [3,1,4]. The symmetry lines are denoted by white dash-dotted lines.

and its conjugate to generate the axisymmetric component. The most dominant frequency triads are (0.4,0.4,0.8), (1.2,-0.4,0.8), (0.4,-0.4,0.0) and their symmetric counterparts, for example, (-0.4,1.2,0.8), and (0.4,-1.2,-0.8). Similarly the self-interaction of the helical component generates peaks at the same frequency triads. For the azimuthal triplet, [2,1,3], the dominant frequency triads are (0.8,-0.4,0.4), (0.8,0.4,1.2), and (-0.8,1.2,0.4). As previously observed in Fig. 2, the odd azimuthal wavenumbers exhibit peaks at odd harmonics and the even azimuthal wavenumbers exhibit peaks at the even harmonics, and the different possible triadic interactions are

$$\text{if } m_1, m_2 \text{ are odd}, \quad (2n_1+1)St_f + (2n_2+1)St_f = 2(n_1+n_2+1)St_f \quad m_3 \text{ is even}, \tag{8}$$

$$\text{if } m_1, m_2 \text{ are even}, \quad (2n_1)St_f + (2n_2)St_f = 2(n_1+n_2)St_f \quad m_3 \text{ is even}, \tag{9}$$

$$\text{if } m_1 \text{ is odd}, m_2 \text{ is even}, \quad (2n_1+1)St_f + (2n_2)St_f = (2(n_1+n_2)+1)St_f \quad m_3 \text{ is odd}, \tag{10}$$

where, $n_1,\ n_2 \in \mathbb{Z}$ are integers. Equations (8)-(10) show that the interaction of two odd or two even wavenumbers always generate peaks at the even harmonics, $\{2St_f, 4St_f, \cdots\}$, whereas the interaction of an odd and even wavenumber generate peaks at the odd harmonics, $\{St_f, 3St_f, 5St_f, \cdots\}$. The most significant frequency triads for the azimuthal triplets, [2,2,4], and [3,1,4] are (1.6,-0.8,0.8), and (0.4,0.4,0.8) which confirm this observation. Note that, the high intensity of the frequency (0,0,0) is ignored while considering the dominant triads because it is an artifact of the spectral leakage of BMD.

The back-scatter phenomenon is not limited to axisymmetrically forced jets but is also present in non-axisymmetrically forced ones. In the case of $m = \pm 1$ forced jets, the back-scatter effect is observed in the azimuthal triplet [2,-1,1] at the frequency triad (0.8,-0.4,0.4), which is not shown here for brevity. In this phenomenon, the second harmonic frequency

$2St_f$ of the azimuthal wavenumber $2m_f$ supplies energy back to the fundamental mode, i.e., the mode corresponding to the frequency St_f and azimuthal wavenumber m_f.

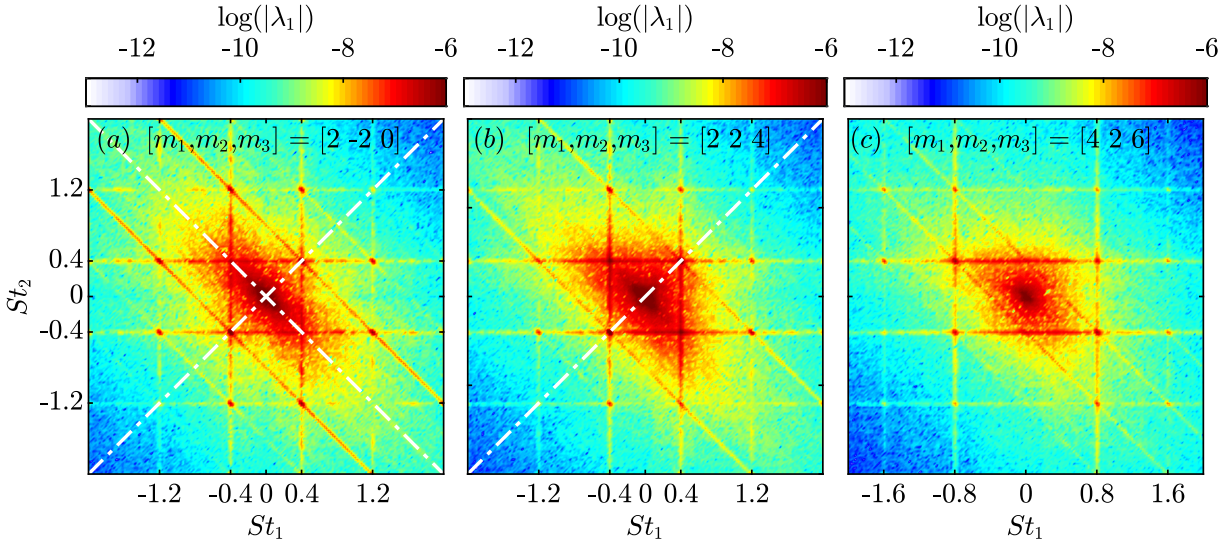

Fig. 5 Cross-BMD spectra that shows the interaction of the azimuthal wavenumbers triads, [m_1, m_2, m_3], for the forced $m = \pm 2$ jet: (a) [2,-2,0]; (b) [2,2,4]; (c) [4,2,6].

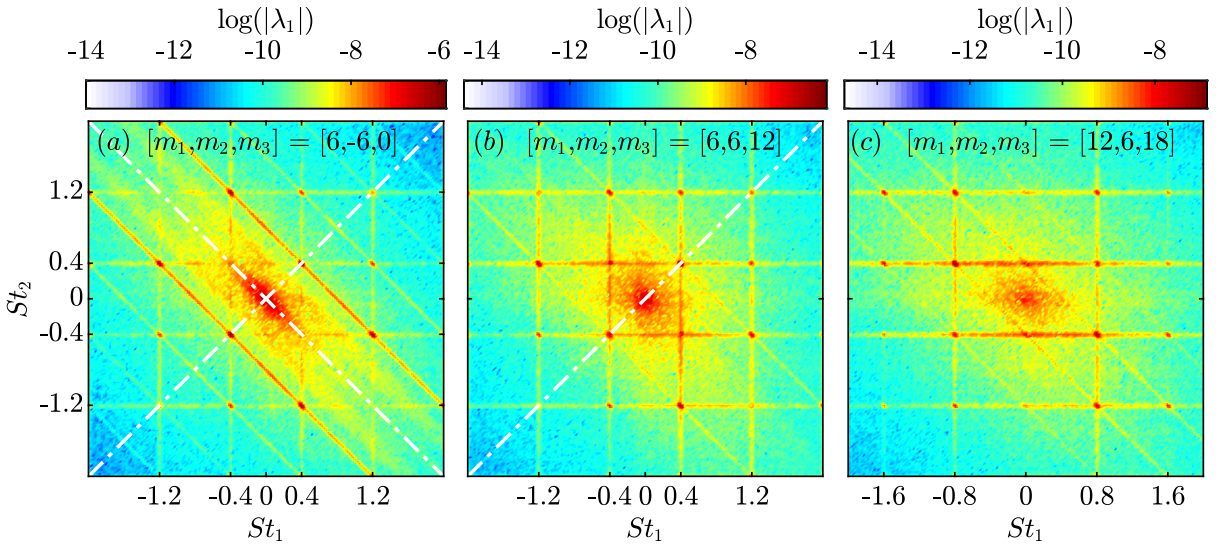

Fig. 6 Cross-BMD spectra that shows the interaction of the azimuthal wavenumbers triads, [m_1,m_2,m_3], for the forced $m = \pm 6$ jet: (a) [6,-6,0]; (b) [6,6,12]; (c) [12,6,18].

Figures 5 and 6 show the cross-BMD spectra for the azimuthal triplets, [2,-2,0], [2,2,4] and [4,2,6] in the $m = \pm 2$-forced jet, and [6,-6,0], [6,6,12] and [12,6,18] in the $m = \pm 6$-forced jet, respectively. As shown in Fig. 2, the non-axisymmetric forcing affects only those azimuthal wavenumbers that are integer multiples of the forcing azimuthal wavenumber. Specifically, the $m = \pm 2$-forced jet excites the azimuthal wavenumbers, $\{\cdots, -4, -2, 0, 2, 4, \cdots\}$, while the $m = \pm 6$-forced jet excites the azimuhtal wavenumbers, $\{\cdots, -12, -6, 0, 6, 12, \cdots\}$. In the $m = \pm 2$ forced case, the peaks (0.4,0.4,0.8), (0.4,-0.4,0.0), and (1.2,-0.4,0.8) in $m = 0$ arise from the interactions between $m = 2$ and $m = -2$ at the forcing frequency and its odd harmonics. Local maxima at the same triads are observed for the self-interaction of $m = 2$ to generate the $m = 4$ component. In the [4,2,6] triplet, even harmonics in $m = 4$ interact with odd harmonics in $m = 2$ to generate odd harmonics in the $m = 6$ component. Similarly, for the $m = \pm 6$ forced jet, the dominant azimuthal triplets are [6,-6,0], [6,6,12], and [12,6,18]. The first two triplets generate even harmonics,

$\{0, 0.8, 1.6, \cdots, \}$, while the third triplet exhibits peaks at odd harmonics, $\{0.4, 1.2, 2.0, \cdots\}$. The spectra in figures 5(a) and 6(a) are symmetric about the lines $St_1 = \pm St_2$, and the spectra in 5(b) and 6(b) are symmetric about the line $St_1 = St_2$. The spectra in the 5(c) and 6(c), on the other hand, are asymmetric.

The observations of figures 4, 5, and 6 suggest the following trends for a general $m = \pm m_f$-forcing:

1) Even harmonics $\{0, 2St_f, 4St_f, \cdots\}$ are generated from azimuthal triplets of the form $[(2k_1)m_f, (2k_2)m_f, 2(k_1 + k_2)m_f]$ and $[(2k_1 + 1)m_f, (2k_2 + 1)m_f, 2(k_1 + k_2 + 1)m_f]$, where $k_1, k_2 \in \mathbb{Z}$.
2) Odd harmonics $\{St_f, 3St_f, 5St_f, \cdots\}$ arise from azimuthal triads of the form $[(2k_1 + 1)m_f, (2k_2)m_f, (2(k_1 + k_2) + 1)m_f]$.
3) The cross-BMD spectrum of the triads $[m_f, -m_f, 0]$ exhibits four-fold symmetry about the lines $St_1 = \pm St_2$.
4) The cross-BMD spectrum of the triads $[m_f, m_f, 2m_f]$ exhibits two-fold symmetry about the line $St_1 = St_2$.
5) The spectra of other triads, such as $[2m_f, m_f, 3m_f]$, are asymmetric.

Next, we will understand how the actuation of the jet results in the abovementioned triads. To begin, we express the Navier-Stokes equation in the following form:

$$\frac{\mathrm{d}\mathbf{q}}{\mathrm{d}t} = \mathcal{L}\mathbf{q} + Q(\mathbf{q}, \mathbf{q}). \tag{11}$$

Here, $\mathcal{L}$ represents the linear operator, and Q denotes the quadratic nonlinearities. By taking the Reynolds decomposition, $\mathbf{q}(\mathbf{x}, t) = \bar{\mathbf{q}}(\mathbf{x}) + \mathbf{q}'(\mathbf{x}, t)$, and substituting it into the equation (11), we obtain:

$$\frac{\mathrm{d}\mathbf{q}'}{\mathrm{d}t} = \mathcal{L}_{\bar{\mathbf{q}}}\mathbf{q}' + Q(\mathbf{q}', \mathbf{q}') \tag{12}$$

where, $\mathcal{L}_{\bar{\mathbf{q}}} = \mathcal{L} + Q(\bar{\mathbf{q}}, \cdot) + Q(\cdot, \bar{\mathbf{q}})$. When the jet is forced at an angular frequency of ω_f and azimuthal wavenumbers $\pm m_f$, the complex representation of the boundary forcing in equation (7b) is expressed as:

$$\mathbf{q}'_f \propto \left(e^{-i(\omega_f t - m_f \theta)} + e^{-i(\omega_f t + m_f \theta)} \right) + \text{c.c.} \tag{13}$$

At the n-th harmonic angular frequency, $n\omega_f$, the temporal Fourier decomposition of the equation can be written as

$$in\omega_f \hat{\mathbf{q}}_{n,m} = \mathcal{L}_{\bar{\mathbf{q}}}\hat{\mathbf{q}}_{n,m} + Q_{n,m}, \tag{14}$$

where,

$$Q_{n,m} = \begin{cases} \sum_l \sum_p Q(\hat{\mathbf{q}}_{l,p}, \hat{\mathbf{q}}_{n-l,m-p}) & \text{if } n,m \text{ are even or } n,m \text{ are odd} \\ 0 & \text{otherwise,} \end{cases} \tag{15}$$

denotes the non-linear interactions that result in the n-th harmonic angular frequency and the m-th azimuthal wavenumber. Here, in $\hat{\mathbf{q}}_{l,p}$, the first subscript denotes the frequency index, and the second subscript denotes the azimuthal wavenumber index.

For example, the triadic interactions that result in the second harmonic frequency can be written as:

$$Q_{2,0} = Q(\hat{\mathbf{q}}_{1,\pm1}, \hat{\mathbf{q}}_{1,\mp1}) + Q(\hat{\mathbf{q}}_{3,\pm1}, \hat{\mathbf{q}}_{-1,\mp1}) + Q(\hat{\mathbf{q}}_{4,\pm2}, \hat{\mathbf{q}}_{-2,\mp2}) + \cdots, \tag{16}$$
$$Q_{2,\pm1} = 0, \tag{17}$$
$$Q_{2,\pm2} = Q(\hat{\mathbf{q}}_{1,\pm1}, \hat{\mathbf{q}}_{1,\pm1}) + Q(\hat{\mathbf{q}}_{3,\pm3}, \hat{\mathbf{q}}_{-1,\mp1}) + Q(\hat{\mathbf{q}}_{4,\pm4}, \hat{\mathbf{q}}_{-2,\mp2}) + \cdots, \tag{18}$$
$$Q_{2,\pm3} = 0. \tag{19}$$

Similarly for the third harmonic frequency,

$$Q_{3,0} = 0, \tag{20}$$
$$Q_{3,\pm1} = Q(\hat{\mathbf{q}}_{1,\mp1}, \hat{\mathbf{q}}_{2,\pm2}) + Q(\hat{\mathbf{q}}_{2,\pm2}, \hat{\mathbf{q}}_{1,\mp1}) + Q(\hat{\mathbf{q}}_{4,\pm4}, \hat{\mathbf{q}}_{-1,\mp3}) + \cdots, \tag{21}$$
$$Q_{3,\pm2} = 0, \tag{22}$$
$$Q_{3,\pm3} = Q(\hat{\mathbf{q}}_{2,\pm2}, \hat{\mathbf{q}}_{1,\pm1}) + Q(\hat{\mathbf{q}}_{4,\pm4}, \hat{\mathbf{q}}_{-1,\mp1}) + Q(\hat{\mathbf{q}}_{5,\pm5}, \hat{\mathbf{q}}_{-2,\mp2}) + \cdots. \tag{23}$$

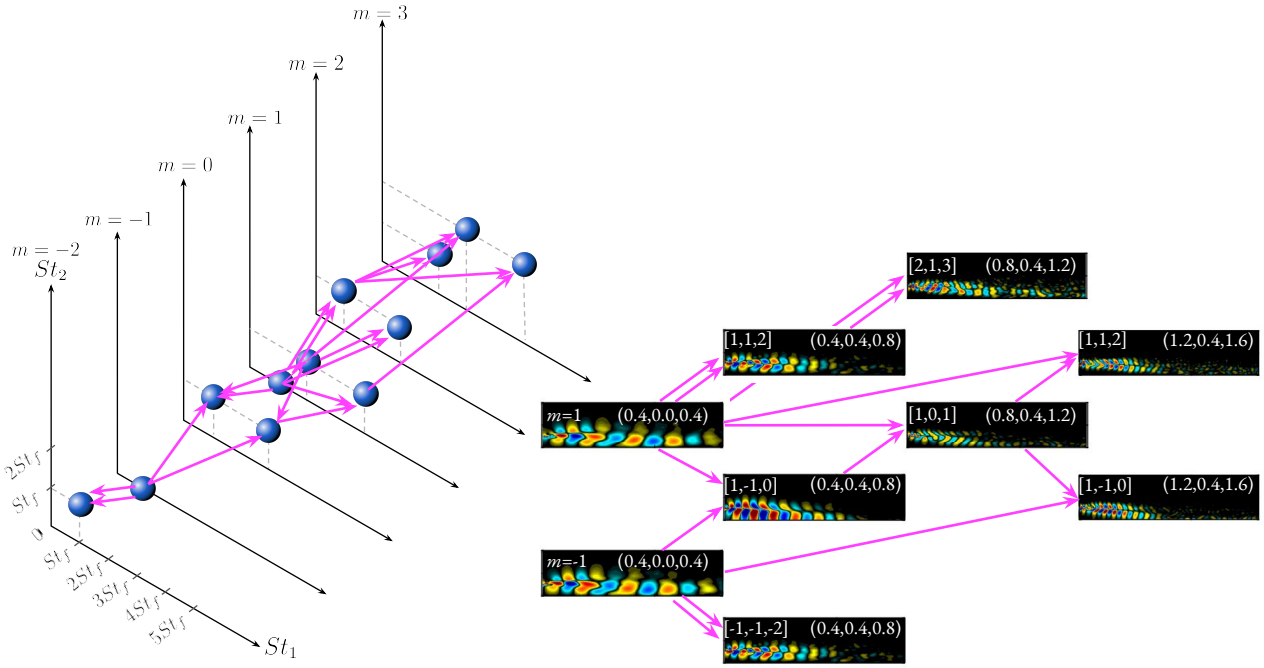

Fig. 7 Example of a forward cascade of triads for the $m = \pm 1$-forced jet.

Equations (16) - (23) demonstrate that the even harmonics are present in the even integer multiples of m_f, while the odd harmonics are present in the odd integer multiples of m_f. This process can be extended to higher harmonics. These equations explain our findings made in context of figures 2, 4, 5, 6.

Fig. 7 shows the spatial structures involved in the cascade of triads for the $m = \pm 1$-forced jet. The BMD modes in the frequency range $St_f \leqslant St_1 \leqslant 3St_f$ and the azimuthal wavenumber range $-1 \leqslant m_1 \leqslant 2$ are visualized here. The forcing initiates the cascade, where $m = 1, St = 0.4$ and $m = -1, St = 0.4$ can undergo two possible interactions: (i) they can interact with each other to generate the $m = 0, St = 0.8$ mode through the wavenumber triad $[m_1, m_2, m_3] = [-1, 1, 0]$ and the frequency triad $(St_1, St_2, St_3) = (0.4, 0.4, 0.8)$; (ii) each of them can self-interact to result in $m = 2, St = 0.8$ or $m = -2, St = 0.8$. The generated modes (second column from the left) then interact with fundamental forcing modes to produce higher harmonics, such as the triad $[2, 1, 3]$, (0.8, 0.4, 1.2). Similarly, the cascade can be extended to higher frequencies and azimuthal wavenumbers. The cascade for $m_3 < 0$ is symmetric to $m_3 > 0$ and is not shown for brevity. Inspecting the modes reveals that the sum interactions in the frequency space create spatial structures with smaller wavelengths, while the sum interactions in the azimuthal wavenumber space result in modes with a larger swirl. An illustration of the cascade in the form of a directed acyclic graph is shown on the left in Fig. 7. Note that the cascade of triads shown in Fig. 7 is one of the many possible pathways of energy transfer.

Fig. 8 depicts the cascade of triads generated by the $m = \pm 6$-forcing, similar to Fig. 7. The major difference is that the azimuthal wavenumbers $\{\cdots, -2, -1, 0, 1, 2, \cdots\}$ are replaced by $\{\cdots, -12, -6, 0, 6, 12, \cdots\}$, i.e., the odd and even integers are replaced by the odd and even integer multiples of 6. The higher azimuthal forcing actuates the spatial structures that are near the nozzle's exit. The BMD mode resulting from the self-interaction of the forcing, [6,6,12] and (0.4,0.4,0.8), is also localized to the vicinity of the nozzle's lip. Though the overall trends are similar, the BMD modes corresponding to the $m = \pm 6$ forcing exhibit greater swirl compared to the modes of the $m = \pm 1$ forcing. An interesting observation is that the BMD modes associated with the frequency triads (0.4, 0.4, 0.8) and (1.2, 0.4, 1.6) in the wavenumber triplet [6, -6, 0] resemble the modes associated with the same frequency triads in the wavenumber triplet [1, -1, 0] for the $m = \pm 1$-forced jet. This indicates that the different $m = \pm m_f$ forcings generate the same spatial structures in the wavenumber triplet $[m_f, -m_f, 0]$.

V. Summary and Conclusion

Large-eddy simulations of unforced and forced jets are performed and validated with companion experiments. The jets are forced at a frequency of $St = 0.4$ and azimuthal wavenumbers, $m = 0$, $m = \pm 1$, $m = \pm 2$, and $m = \pm 6$. BMD

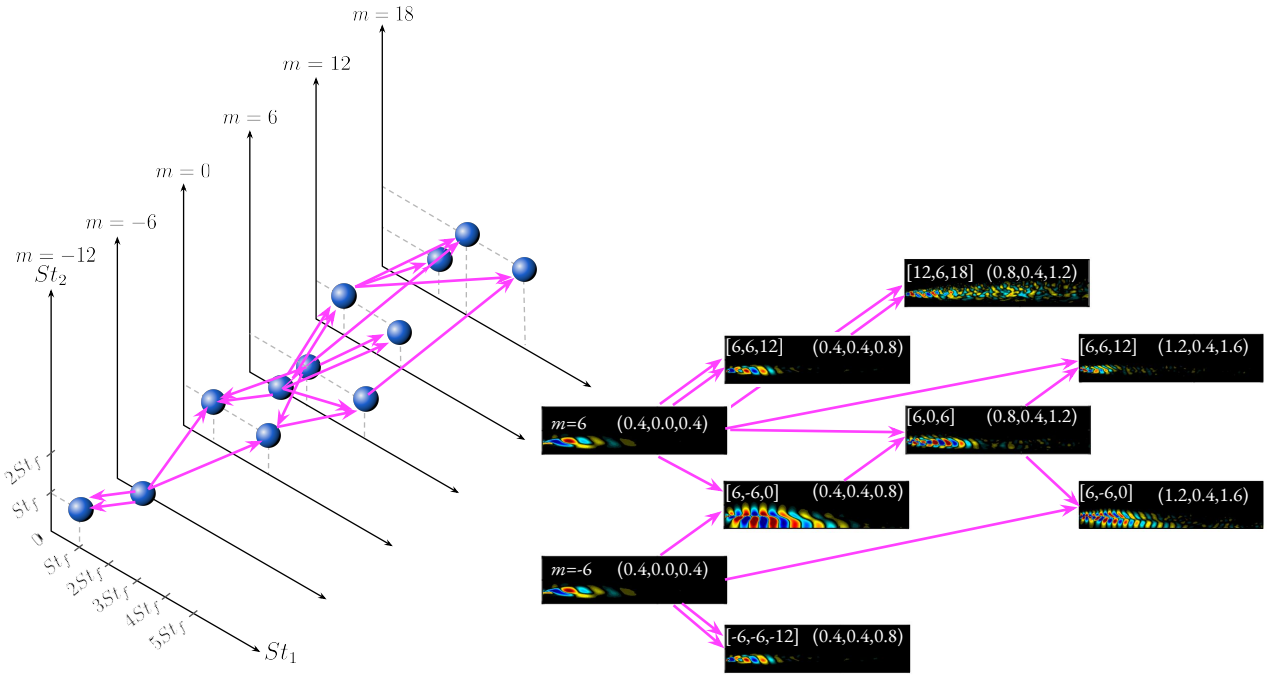

Fig. 8 Example of a forward cascade of triads for the $m = \pm 6$-forced jet.

and cross-BMD are performed to investigate the triadic interaction in the forced jets. The analysis reveals that the triadic interactions due to the actuation occur only in the $m = 0$ component for the axisymmetrically forced jet, whereas the triadic interactions occur across different azimuthal wavenumbers for the non-axisymmetrically forced jet. In the case of the $m_f = 0$ jet, the prominent azimuthal wavenumber triplet is [0, 0, 0]. The two most dominant triads are due to the self-interaction of the forcing frequency, $[St_f, St_f, 2St_f]$, and due to harmonic-fundamental difference interaction, $(2St_f, -St_f, St_f)$, that scatters energy back into the fundamental. On the other hand, for the non-axisymmetrically forced jets, different wavenumber triplets are important, such as, $[m_f, -m_f, 0]$, $[m_f, m_f, 2m_f]$, and $[2m_f, m_f, 3m_f]$. The cascade of triads is initiated by the self-interaction of the fundamental frequency, $(St_f, St_f, 2St_f)$ in the wavenumber triplets $[m_f, -m_f, 0]$, $[m_f, m_f, 2m_f]$. The resulting triads then interact with the forcing modes to generate the odd harmonic frequencies in the odd integer multiples of the wavenumber forcing. For instance, the odd harmonic frequency $3St_f$ at $3m_f$ is created through the frequency triad $(2St_f, St_f, 3St_f)$ and the wavenumber triad $[2m_f, m_f, 3m_f]$. The cascade proceeds in a similar way to generate the even harmonics in the even integer multiples of the wavenumber forcing. As an example, the $3St_f$ at $3m_f$ interacts with St_f at m_f to generate the fourth harmonic frequency, $4St_f$, in the fourth integer multiple of the forcing wavenumber, $4m_f$.

Acknowledgments

AN and OTS gratefully acknowledge support from the Office of Naval Research grant N00014-20-1-2311 and National Science Foundation grant CBET 2046311.

References

[1] Crow, S., and Champagne, F., "Orderly structure in jet turbulence," *J. Fluid Mech.*, Vol. 48, No. 3, 1971, pp. 547–591.

[2] Jordan, P., and Colonius, T., "Wave packets and turbulent jet noise," *Annu. Rev. Fluid Mech.*, Vol. 45, 2013, pp. 173–195.

[3] Zaman, K. B. M. Q., and Hussain, A. K. M. F., "Vortex pairing in a circular jet under controlled excitation. Part 1. General jet response," *J. Fluid Mech.*, Vol. 101, No. 3, 1980, pp. 449–491.

[4] Hussain, A. K. M. F., and Zaman, K. B. M. Q., "Vortex pairing in a circular jet under controlled excitation. Part 2. Coherent structure dynamics," *J. Fluid Mech.*, Vol. 101, No. 3, 1980, pp. 493–544.

[5] Zaman, K. B. M. Q., and Hussain, A. K. M. F., "Turbulence suppression in free shear flows by controlled excitation," *J. Fluid Mech.*, Vol. 103, 1981, pp. 133–159.

[6] Laufer, J., and Yen, T. C., "Noise generation by a low-Mach-number jet," *J. Fluid Mech.*, Vol. 134, 1983, pp. 1–31.

[7] Morrison, G. L., and McLaughlin, D. K., "Noise generation by instabilities in low Reynolds number supersonic jets," *J. Sound Vib.*, Vol. 65, No. 2, 1979, pp. 177–191.

[8] Hussain, A. K. M. F., and Zaman, K. B. M. Q., "The 'preferred mode'of the axisymmetric jet," *J. Fluid Mech.*, Vol. 110, 1981, pp. 39–71.

[9] Raman, G., and Rice, E., "Axisymmetric jet forced by fundamental and subharmonic tones," *AIAA J.*, Vol. 29, No. 7, 1991, pp. 1114–1122.

[10] Husain, H., and Hussain, F., "Experiments on subharmonic resonance in a shear layer," *J. Fluid Mech.*, Vol. 304, 1995, pp. 343–372.

[11] Broze, G., and Hussain, F., "Nonlinear dynamics of forced transitional jets: periodic and chaotic attractors," *J. Fluid Mech.*, Vol. 263, 1994, pp. 93–132.

[12] Cohen, J., and Wygnanski, I., "The evolution of instabilities in the axisymmetric jet. Part 2. The flow resulting from the interaction between two waves," *J. Fluid Mech.*, Vol. 176, 1987, pp. 221–235.

[13] Long, T. A., and Petersen, R. A., "Controlled interactions in a forced axisymmetric jet. Part 1. The distortion of the mean flow," *J. Fluid Mech.*, Vol. 235, 1992, pp. 37–55.

[14] Corke, T. C., and Kusek, S. M., "Resonance in axisymmetric jets with controlled helical-mode input," *J. Fluid Mech.*, Vol. 249, 1993, pp. 307–336.

[15] Samimy, M., Kim, J. H., Kastner, J., Adamovich, I., and Utkin, Y., "Active control of high-speed and high-Reynolds-number jets using plasma actuators," *J. Fluid Mech.*, Vol. 578, 2007, pp. 305–330.

[16] Reynolds, W. C., Parekh, D. E., Juvet, P. J. D., and Lee, M. J. D., "Bifurcating and blooming jets," *Annu. Rev. Fluid Mech.*, Vol. 35, No. 1, 2003, pp. 295–315.

[17] Wu, X., and Huerre, P., "Low-frequency sound radiated by a nonlinearly modulated wavepacket of helical modes on a subsonic circular jet," *J. Fluid Mech.*, Vol. 637, 2009, pp. 173–211.

[18] Suponitsky, V., Sandham, N. D., and Morfey, C. L., "Linear and nonlinear mechanisms of sound radiation by instability waves in subsonic jets," *J. Fluid Mech.*, Vol. 658, 2010, pp. 509–538.

[19] Schmidt, O. T., "Bispectral mode decomposition of nonlinear flows," *Nonlinear Dyn.*, Vol. 102, No. 4, 2020, pp. 2479–2501.

[20] Goparaju, H., and Gaitonde, D. V., "Role of entropic instabilities in laminar-turbulent transition on a blunted flat plate," *Phys. Rev. Fluids*, Vol. 7, No. 10, 2022, p. 103901.

[21] Maia, I., Jordan, P., Heidt, L., Colonius, T., Nekkanti, A., and Schmidt, O. T., "Nonlinear dynamics of forced wavepackets in turbulent jets," *AIAA Aviation 2021 Forum*, 2021, p. 2277.

[22] Nekkanti, A., Maia, I., Jordan, P., Heidt, L., Colonius, T., , and Schmidt, O. T., "Triadic nonlinear interactions and acoustics of forced versus unforced turbulent jets," *Twelveth International Symposium on Turbulence and Shear Flow Phenomena (TSFP12)*, Osaka, Japan (Online), July 19-22, 2022.

[23] Moczarski, L., Treleaven, N. C., Oberleithner, K., Schmidt, S., Fischer, A., and Kaiser, T. L., "Interaction of multiple linear helical modes in the turbulent flow field of an industrial fuel injection system," *AIAA SciTech 2022 Forum*, 2022, p. 1061.

[24] Nekkanti, A., Nidhan, S., Schmidt, O. T., and Sarkar, S., "Large-scale streaks in a turbulent bluff body wake," *arXiv preprint arXiv:2304.08679*, 2023.

[25] Patel, H. D., and Yeh, C. A., "Modal analysis for three-dimensional instability coupling mechanisms in turbulent wake flows over an airfoil," *AIAA SCITECH 2023 Forum*, 2023, p. 1987.

[26] Heidt, L., and Colonius, T., "Spectral proper orthogonal decomposition of harmonically forced turbulent flows," *arXiv preprint*, 2023.

[27] Welch, P., "The use of fast Fourier transform for the estimation of power spectra: a method based on time averaging over short, modified periodograms," *IEEE Trans. Audio Electroacoust.*, Vol. 15, No. 2, 1967, pp. 70–73.

[28] Maia, I. A., Jordan, P., Cavalieri, A. V. G., Martini, E., and Silvestre, F., "Closed-loop control of forced turbulent jets," *arXiv preprint arXiv:2009.09299*, 2020.

[29] Maia, I. A., Jordan, P., Cavalieri, A. V. G., Martini, E., Sasaki, K., and Silvestre, F. J., "Real-time reactive control of stochastic disturbances in forced turbulent jets," *Phys. Rev. Fluids*, Vol. 6, No. 12, 2021, p. 123901.

[30] Maia, I. A., Jordan, P., and Cavalieri, A. V. G., "Wave cancellation in jets with laminar and turbulent boundary layers: The effect of nonlinearity," *Phys. Rev. Fluids*, Vol. 7, No. 3, 2022, p. 033903.

[31] Brès, G. A., Ham, F. E., Nichols, J. W., and Lele, S. K., "Unstructured large-eddy simulations of supersonic jets," *AIAA Journal*, 2017, pp. 1164–1184.

[32] Brès, G. A., Jordan, P., Jaunet, V., Le Rallic, M., Cavalieri, A. V. G., Towne, A., Lele, S. K., Colonius, T., and Schmidt, O. T., "Importance of the nozzle-exit boundary-layer state in subsonic turbulent jets," *J. Fluid Mech.*, Vol. 851, 2018, pp. 83–124.

[33] Vreman, A., "An eddy-viscosity subgrid-scale model for turbulent shear flow: Algebraic theory and applications," *Phys. Fluids*, Vol. 16, No. 10, 2004, pp. 3670–3681.

[34] Bodart, J., and Larsson, J., "Wall-modeling in large eddy simulation: length scales, grid resolution, and accuracy," *Annual research briefs*, 2012, pp. 229–240.

[35] Kawai, S., and Larsson, J., "Wall-modeling in large eddy simulation: Length scales, grid resolution, and accuracy," *Phys. Fluids*, Vol. 24, No. 1, 2012, p. 015105.

[36] Heidt, L., Colonius, T., Nekkanti, A., Schmdit, O., Maia, I., and Jordan, P., "Analysis of forced subsonic jets using spectral proper orthogonal decomposition and resolvent analysis," *AIAA Aviation 2021 Forum*, 2021, p. 2108.